Comparison of Mean Properties of Simulated Convection in a Cloud-Resolving Model with Those Produced by Cumulus Parameterization

J. Dudhia
Mesoscale and Microscale Meteorology Division
National Center for Atmospheric Research
Boulder, Colorado

D. B. Parsons
Atmospheric Technology Division
National Center for Atmospheric Research
Boulder, Colorado

Introduction

An Intensive Observation Period (IOP) of the Atmospheric Radiation Measurement (ARM) Program took place at the Southern Great Plains (SGP) Cloud and Radiation Testbed (CART) site from June 16-26, 1993.

The National Center for Atmospheric Research (NCAR)/Penn State Mesoscale Model (MM5) has been used to simulate this period on a 60-km domain with 20- and 6.67-km nests centered on Lamont, Oklahoma. Simulations are being run with data assimilation by the nudging technique (Kuo and Guo 1989; Stauffer and Seaman 1990) to incorporate upper-air and surface data from a variety of platforms. The model maintains dynamical consistency between the fields, while the data correct for model biases that may occur during long-term simulations and provide boundary conditions. For the work reported here the Mesoscale Atmospheric Prediction System (MAPS) of the National Ocean and Atmospheric Administration (NOAA) 3-hourly analyses were used to drive the 60-km domain while the inner domains were unforced. A continuous 10-day period was simulated.

Overview

One goal of the ARM Program is to improve general circulation models (GCMs) by obtaining detailed meteorological information in limited areas of under 200 km square and comparing GCM parameterizations with the mean radiative and convective properties in such areas. Typical GCM grid boxes are 100-200 km square, but there is in reality much structure at smaller scales that is represented by their parameterizations. Meteorological observations alone cannot represent this structure, so we use a full-physics mesoscale model forced by large-scale tendencies to give as complete a picture of the sub-100-km scale structures as possible.

Here we will concentrate on one day (June 24) when a cold front entered the domain. The convection associated with this front is simulated at several resolutions and with various cumulus schemes on the climate-scale model resolution to evaluate whether these schemes can represent the model behavior at high resolution where the clouds are resolved.

The MM5 Model

The model features and options used in this study are as follows. Equations are for nonhydrostatic, compressible motion, in terrain-following coordinates with a polar-stereographic map projection. Prognostic equations exist for wind components, vertical velocity, pressure perturbation, temperature, water vapor, ground temperature, and microphysical water and ice content variables. It has an upper radiative boundary condition, relaxation lateral boundary conditions, and interactive two-way nesting.

The model includes microphysics with cloud, rain, snow/graupel, and ice processes on all domains' resolved scales. The Grell cumulus parameterization scheme is adopted only on the 20-km and coarser domains. The Blackadar high-resolution planetary boundary layer and a

surface energy budget calculation are used. There is also an atmospheric longwave and shortwave radiation scheme interacting with model clouds and land surface.

Domain and Simulations

Figure 1 shows the areas covered by the three MM5 domains. The 60-km domain coincides with the MAPS domain. The inner 6.67-km domain is centered on a profiler hexagon of the demonstration network around Lamont, Oklahoma, and covers a 480-km square.

Concentrating on 24 June, a series of test simulations was run to compare convection at several grid sizes. A simulation in which the 6.67-km domain was switched off at 00Z/24th was run 24 hours with the Grell scheme with 20-km grid size, and similarly one was run at just 60-km resolution. A further pair of simulations used 60-km initial conditions at 00Z/24th degraded to 180-km grid size, using 1) the Grell scheme, and 2) the CCM2 convective adjustment scheme.

However, 6.67 km is probably not sufficient to resolve updrafts well, so another experiment was run from 12Z/24th for 12 hours at 2.22 km nested in the center of the 6.67-km domain. This serves as a test of the explicit 6.67-km simulation, and the highly resolved cloud structures in a 160-km square will be compared to the representations on coarser meshes. Here we will present the mean effects of convection on the 160- km scale.

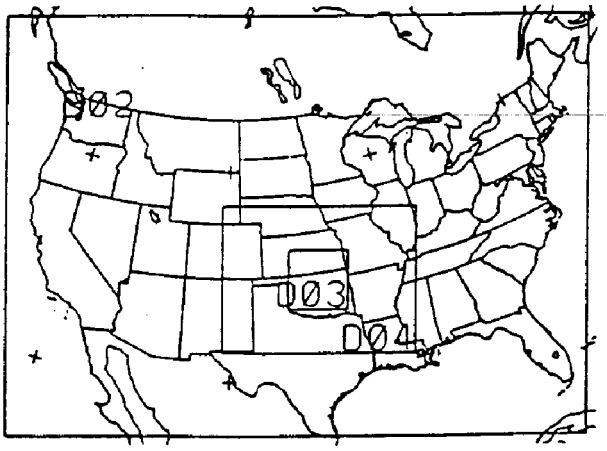

Figure 1. Domains for the simulations (60 km, 20 km, 6.67 km).

The Cold Front of June 24, 1993

Figure 2a shows a cold front across Oklahoma/Kansas around 18Z 24 June 1993. This front had moved into Oklahoma over the previous 6-12 hours and became stationary over the CART site. The radar summary (Figure 2b) shows that convergence ahead of the front was capable of triggering convection over northern Oklahoma and southern Kansas. The modeled surface winds and temperature at 18Z on June 24 are shown on Figure 3.

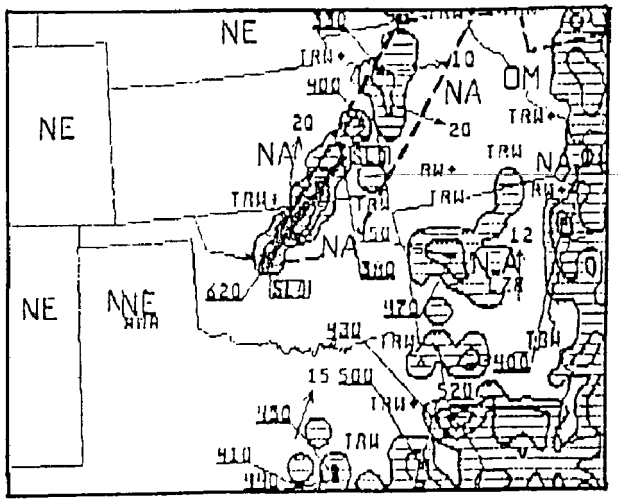

Figure 2a. Radar summary for 1935Z 24 June 1993.

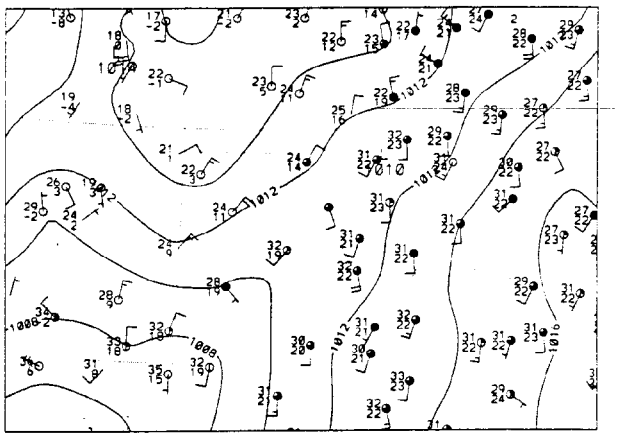

Figure 2b. Surface pressure analysis, wind and temperature observations for 18Z 24 June 1993. Contour interval 2 hPa, wind barbs in m/s.

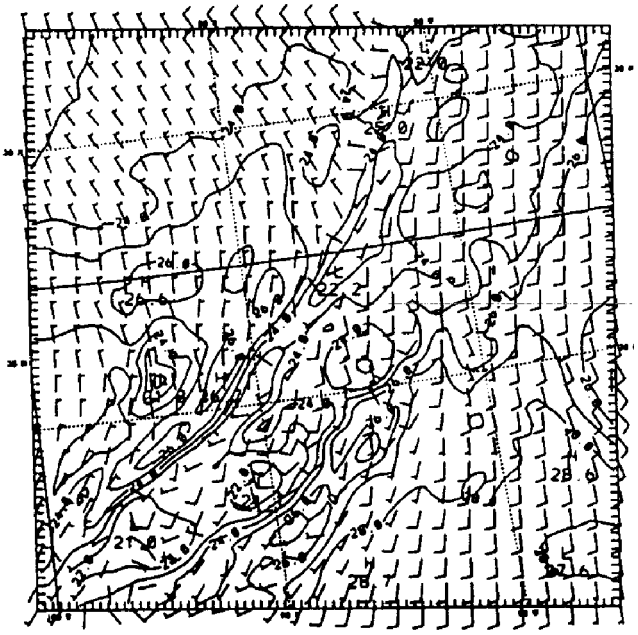

Figure 3. Surface wind and temperature for model 6.67-km domain for 18Z 24 June 1993. Contour interval 1 C, wind barbs in m/s.

Results

Resolution Dependence of Rainfall

Figure 4 shows how the rainfall at 18Z/24th depends on the grid resolution for the various experiments at 60 km and 2.22 km. Resolution experiments were run at 180-, 60-, 20-, 6.67-, and 2.22-km grid size. It can be seen that while the finer meshes contain active convection (Figure 4a) the coarser resolution (Figure 4b) misses it.

Mean Properties of the 2.22-km Simulation

Figure 5 shows domain averages of the heating and moistening rates in the 2.22-km domain, depicted as time-pressure plots over the 12-hour period and from 100 to 1000 hPa levels. These are expressed in terms of

$$Q_1 = \frac{\overline{\partial T}}{\partial t} + \overline{u}\frac{\overline{\partial T}}{\partial x} + \overline{v}\frac{\overline{\partial T}}{\partial y} + \overline{w}\frac{\overline{\partial T}}{\partial z} + \frac{g}{c_p}\overline{w}$$

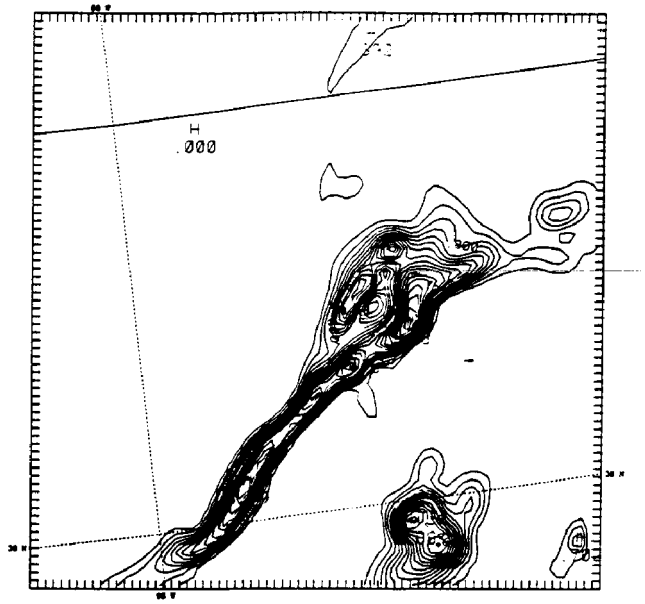

Figure 4a. 2.22-km domain's rainwater at lowest level. Contour interval 0.2 g/kg.

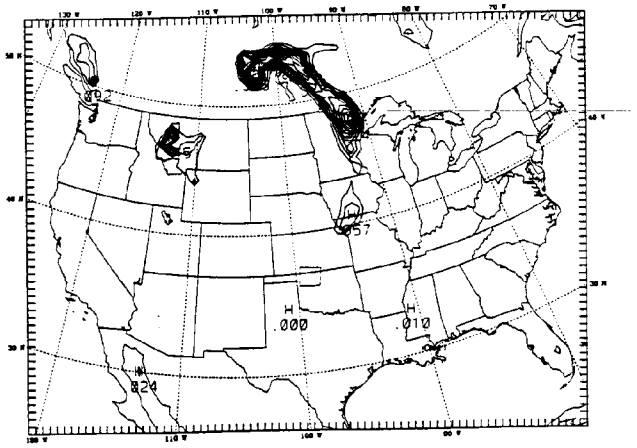

Figure 4b. 60-km domain's rainwater at lowest level. Contour interval 0.02 g/kg. Square marks location of 2.22-km domain.

$$\frac{L_v}{c_p} Q_2 = \frac{L_v}{c_p}\left[\frac{\overline{\partial q}}{\partial t} + \overline{u}\frac{\overline{\partial q}}{\partial x} + \overline{v}\frac{\overline{\partial q}}{\partial y} + \overline{w}\frac{\overline{\partial q}}{\partial z}\right]$$

and are useful measures of convective activity since Q_1 and Q_2 are dependent upon the condensational heating/drying term and vertical eddy transports of heat/moisture.

Figures 5a and 5b show the high-level apparent heat source and lower apparent moisture sink during the convective stage with the signs reversing in a dissipative stage around 20Z, when evaporation exceeds condensation in the domain

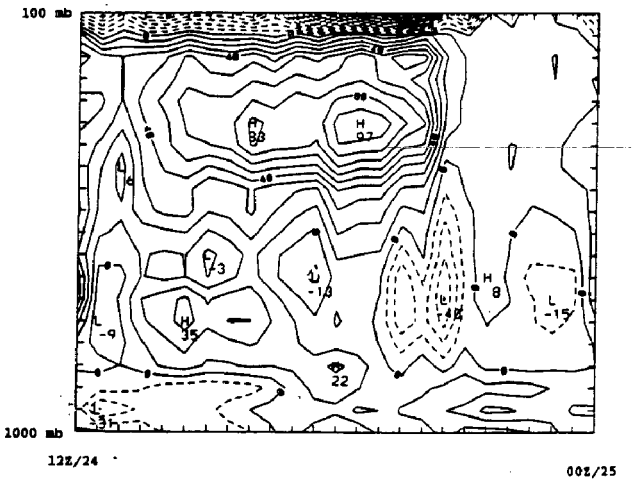

Figure 5a. Pressure versus time plot of the apparent heat source, Q1, between 12Z 24 June and 00Z 25 June 1993, for the 2.22-km domain. Contour interval 10^{-5} K/s.

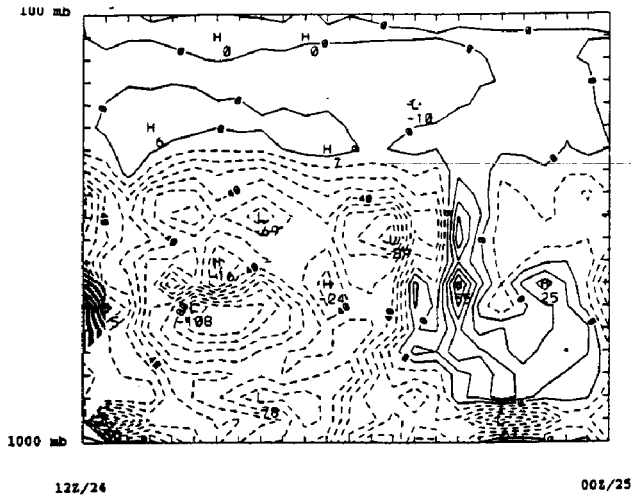

Figure 5b. Pressure versus time plot of the apparent latent heat source, (equation) Q2, between 12Z 24 June and 00Z 25 June 1993, for the 2.22-km domain. Contour interval 10^{-5} K/s.

average. Maximum values correspond to 10 K/d in sensible and latent heating due to the convective processes in the area.

Mean Mass Fluxes of the Simulations

Figure 6 shows how the mean mass flux, taken over the area of the 2.22-km domain, decreases as the grid size gets larger. This is consistent with the reduced rainfall rates at low resolutions. Figure 6a shows that the mean mass flux over the 12-hour period, M = (equation), reaches nearly 0.2 kg m^{-2} s^{-1} for the 2.22-km domain average, but at 60 km (Figure 6b). it is only about 0.04 kg m^{-2} s^{-1} averaged over the same area.

This emphasizes that to evaluate convective parameterizations, one must use cloud-resolving models because it is only at high resolution that some convection is triggered, while the current cumulus schemes underestimate vertical mass flux and rainfall as a result of failing to trigger.

In this case, there was a stable layer ahead of the front that probably inhibited the parameterized convection, whereas the resolved lifting at fine resolution was sufficient to overcome this inhibition.

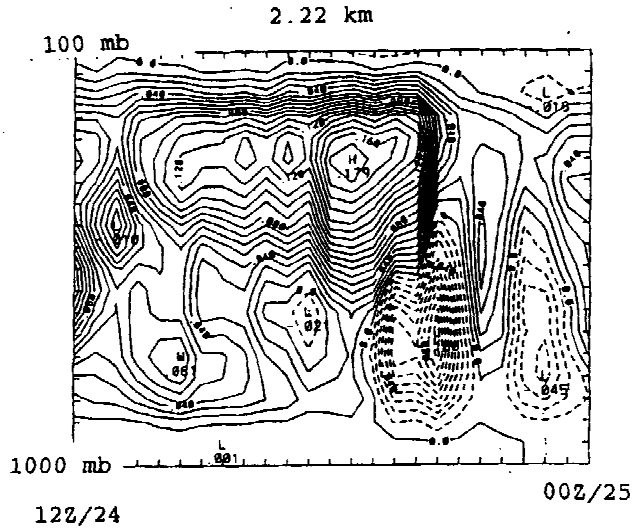

Figure 6a. Pressure versus time plot of mean mass flux, M, in 2.22-km domain, between 12Z 24 June and 00Z 25 June 1993. Contour interval 0.01 kg m^{-2} s^{-1}.

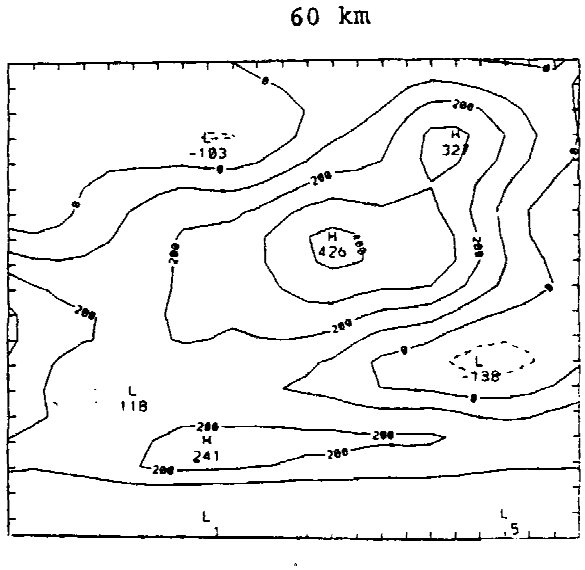

Figure 6b. Pressure versus time plot of mean mass flux, M-, in 60-km domain, between 12Z 24 June and 00Z 25 June 1993. Contour interval 0.01 kg m^{-2} s^{-1}.

Further Work

Further work in this area will include the following:

1. Enhance high-resolution simulations with assimilation of more local data (e.g., profiler network). This could allow a more accurate simulation of the rainfall pattern associated with the front.

2. Evaluate cloud fractional coverage versus that predicted in GCMs' radiation schemes. Determine mean radiative properties of resolved cloud fields.

3. Evaluate mean boundary-layer fluxes in high-resolution models and compare with GCMs.

4. Improve cumulus parameterization such that it can reproduce a cloud-resolving model's rainfall/mass flux, possibly by modifying the scheme's initiation conditions or by trying a variety of schemes.

References

Kuo, Y.-H., and Y.-R. Guo. 1989. Dynamic initialization using observations from a hypothetical network of profiles, *Mon. Wea. Rev.*, **117**, 1975-1998.

Stauffer, D. R., and N. L. Seaman. 1990. Use of four-dimensional data assimilation in a limited area mesoscale model. Part I: Experiments with synoptic-scale data, *Mon. Wea. Rev.*, **118**, 1250-1277.